Applied Surface Science 379 (2016) 384–394

Contents lists available at ScienceDirect

Applied Surface Science

journal homepage: www.elsevier.com/locate/apsusc

Unraveling the role of support surface hydroxyls and its effect on the selectivity of C_2 species over Rh/γ-Al_2O_3 catalyst in syngas conversion: A theoretical study

Riguang Zhang, Tian Duan, Baojun Wang*, Lixia Ling

Key Laboratory of Coal Science and Technology of Ministry of Education and Shanxi Province, Taiyuan University of Technology, Taiyuan 030024, Shanxi, China

ARTICLE INFO

Article history:
Received 13 November 2015
Received in revised form 3 March 2016
Accepted 15 April 2016
Available online 19 April 2016

Keywords:
Rh/γ-Al_2O_3
Syngas conversion
Hydroxylation
C_2 oxygenates
C_2 hydrocarbons
Density functional theory

ABSTRACT

The supported Rh-based catalysts exhibit the excellent catalytic performances for syngas conversion to C_2 species. In this study, all possible elementary steps leading to C_2 species from syngas have been explored to identify the role of support and its surface hydroxyls over Rh/γ-Al_2O_3 catalyst; Here, the results are obtained using density functional theory (DFT) method. Two models: Rh4 cluster supported on the dry γ-Al_2O_3(110) surface, D(Rh4), and on the hydroxylated γ-Al_2O_3(110) surface, H(Rh4), have been used to model Rh/γ-Al_2O_3 catalyst. Our results show that CO prefers to be hydrogenated to CHO, subsequently, starting from CHO species, CH and CH_2 species are the dominate monomers among CH_x(x = 1–3) species rather than CH_3 and CH_3OH on D(Rh4) and H(Rh4) surfaces, suggesting that γ-Al_2O_3-supported Rh catalyst exhibits the high selectivity towards CH_x formation compared to the pure Rh catalyst. On the other hand, D(Rh4) is more favorable for C_2 hydrocarbon (C_2H_2) formation, whereas H(Rh4) surface easily produces C_2 hydrocarbon (C_2H_2) and C_2 oxygenates (CHCO,CH_2CHO), indicating that the surface hydroxyls of support can affect the selectivity of C_2 species over Rh/γ-Al_2O_3 catalyst in syngas conversion. Moreover, compared to the pure Rh(111) surface, Rh/γ-Al_2O_3 catalyst can achieve the excellent catalytic performances for syngas conversion to C_2 species.

1. Introduction

It is well known that the supported Rh-based catalysts exhibit excellent performances for the formation of C_2 species from syngas ($CO + H_2$) (typically referred to as acetaldehyde, ethanol, etc.) [1–10]. Up to now, extensive efforts have been devoted to investigate the effect of supports on the selectivity of CO hydrogenation over the supported Rh-based catalysts, in which a large number of studies have been focused on SiO_2 supports due to its high surface area, high porosity and good stability [4,8,9,11–16], in addition, previous studies by Burch et al. [17] have presented that the reducible metal oxide promoters result in a low selectivity to propane and acetaldehyde but a high selectivity to ethanol; meanwhile, TiO_2 support has also been extensively examined [4,5,14,18,19], suggesting that TiO_2 support can give the highest selectivity for C_2 oxygenates. In addition, the supports La_2O_3 [20], ZrO_2 [21], CeO_2 [22], MgO [23], V_2O_3 [24] and Al_2O_3 [25,26] have been also reported.

For the role of the supports, the supports not only disperse metal particles, but also modify the properties of active metal species through metal-support interactions; meanwhile, previous reports have shown that the selectivity of CO hydrogenation can be significantly influenced by changing the supports [19–23,27]. For example, Katzer et al. [23] have investigated the role of the support in the selectivity of CO hydrogenation over different types of the supported-Rh catalysts, suggesting that CO hydrogenation selectivity to alcohols varies with the basic character of the support; MgO-supported Rh catalyst presents 90% selectivity to methanol, while Rh supported on TiO_2 is in favor of ethanol formation. Meanwhile, the experimental studies by Ichikawa [21] have shown that Rh supported on strongly basic oxides MgO leads to methanol as a major product, however, when Rh deposited on acidic oxides Al_2O_3 and SiO_2, the products are CH_4 and higher hydrocarbons [27]. On the other hand, previous studies [25,28–31] have shown that surface hydroxyls can lead to buildup of the a surface metal monolayer on the oxide support. For example, just because of the low surface density of reactive surface hydroxyl on SiO_2 support,

* Corresponding author at: No. 79 Yingze West Street, Taiyuan 030024, China.
E-mail addresses: wangbaojun@tyut.edu.cn, quantumtyut@126.com (B. Wang).

http://dx.doi.org/10.1016/j.apsusc.2016.04.106
0169-4332/

the close-packed monolayer of the surface metal phase does not appear, whereas, both Al_2O_3 and TiO_2 supports have been reported to have a much higher density of surface hydroxyls, which allows the formation of a close-packed monolayer of the supported metal [25]; thus, the surface hydroxyls of support also affects the particle size and shape of the supported metal and the metal-support interaction, further, it will affect the reactions taking place on the supported catalyst.

Up to now, in syngas conversion, previous studies have reported the effects of surface hydroxyls over TiO_2 support on the selectivity of C_2 oxygenates over Rh/TiO_2 catalysts [5], suggesting that the hydroxylation of TiO_2 surface yields a fairly "inert" support that is much similar to SiO_2 in terms of its effect on selectivity. However, to the best of our knowledge, the effects of surface hydroxyls over Al_2O_3 support on the selectivity of C_2 species including oxygenates and hydrocarbons are still unclear over Rh/Al_2O_3 catalysts; Al_2O_3, especially γ-Al_2O_3, has been widely used as support in heterogeneous catalysis including CO and CO_2 conversion; since metal particles supported on oxides such as γ-Al_2O_3 have been found to be effective for the catalytic conversions of CO [32–34] and CO_2 [35,36], and a good dispersion of metal particles on γ-Al_2O_3 due to high porosity and specific surface area [37–41]; more importantly, for γ-Al_2O_3-supported metal catalysts, the surface of γ-Al_2O_3 will inevitably be hydrated/hydroxylated under the realistic reaction condition, for example, the previous studies by Mei et al. [42] have shown that γ-Al_2O_3(100) surface is expected to be fully dehydrated when the temperature is above 600 K; then, the nature of γ-Al_2O_3 surface will be modified [35,36,43–45]; as a result, the reactions taking place on the supported catalyst will be affected; for example, previous studies [46–48] have probed into the effect of surface hydroxyls on the selectivity of CO_2 hydrogenation to HCOO and CO over Ni/γ-Al_2O_3, Cu/γ-Al_2O_3 and Pd/γ-Al_2O_3 catalysts, respectively, suggesting that the surface hydroxyls of γ-Al_2O_3 can alter the reaction pathway, and ultimately, the activity and selectivity of CO_2 hydrogenation on these catalysts.

Syngas conversion to C_2 species generally involves two key steps, one is the formation of CH_x species including CO direct dissociation into C, followed by C hydrogenation or CO hydrogenation to CH_xO and CH_xOH, followed by the C—O bond cleavage to form CH_x species; the other is the formation of C_2 species by CO/CHO insertion into CH_x to C_2 oxygenates or CH_x coupling to C_2 hydrocarbons [10,49,50]. As a result, the modifications using the different properties of supports usually promote one or two key steps, which can make syngas conversion to the desirable C_2 species. Thus, it is necessary to better understand the role of surface hydroxyls and its effect on the selectivity of C_2 species over Rh/γ-Al_2O_3 catalyst and illustrate the key factors that affect the selectivity of catalysts in syngas conversion; However, the experimental characterization of alumina supported heterogeneous catalysts is rather difficult due to the porosity and disorder of γ-Al_2O_3 support. Therefore, density functional theory (DFT) calculations on the realistic γ-Al_2O_3 model has been employed to obtain the relevant insight into the reaction mechanism of heterogeneous catalysis [37,46–48,51,52].

In this study, we explore all possible elementary steps involving in the formation mechanisms of C_2 species from syngas on Rh/γ-Al_2O_3 catalyst using DFT calculations, which includes two key steps, CH_x(x = 1–3) species formation, C_2 oxygenates and hydrocarbons formations. For γ-Al_2O_3 support, two types of systems: the dry (fully dehydrated) γ-Al_2O_3(110) surface and the partially hydroxylated γ-Al_2O_3(110) surface, have been constructed to reflect the properties of surface hydroxyls of γ-Al_2O_3 support, subsequently, a direct comparison of syngas conversion to C_2 species over the dry and hydroxylated γ-Al_2O_3-supported Rh catalysts can clearly present a clear picture about the effect of surface hydroxyls on the selectivity of the desirable C_2 products. Meanwhile, a detailed characterization of syngas conversion over Rh/γ-Al_2O_3 catalyst at the molecular level will help us better understand the underlying reaction mechanisms, and aid in the elucidation of key factors that affect catalyst performances. Further, an atomic-scale understanding of reaction mechanism would facilitate the design of improved catalysts for syngas conversion.

2. Computational details

2.1. Surface model

The γ-Al_2O_3 structural models have been proposed according to the defective spinel and non-spinel models [51,53–57]. The non-spinel model has been well characterized both experimentally and theoretically [53–57]. Moreover, the non-spinel model produces the diffraction patterns that are close to the characteristic diffraction patterns of γ-Al_2O_3 [56–58]. Thus, the non-spinel γ-Al_2O_3 model has been employed to construct surfaces in the previous studies [46,51,53,59,60], the same size of unit cell as previous studies was used to model γ-Al_2O_3 surface in this study, which is enough for our investigations about syngas conversion to C_2 species. Herein, the (110) surface of γ-Al_2O_3 is chosen according to the fact that the (110) surface accounts for more than 70% of the total surface area, which is expected to dominate the exposed surfaces of γ-Al_2O_3 under the real catalytic conditions [51,61,62].

The dry γ-Al_2O_3(110) surface is modeled by a supercell included a $p(2 \times 1)$ surface unit cell, the vacuum region separating the slabs in the direction perpendicular to the surface direction is set to 12 Å, thus, the dry γ-Al_2O_3(110) surface has a dimension of $8.40 \times 8.07 \times 19.17$ Å. Twelve Al_2O_3 molecular units in the slab are distributed in six layers. On the other hand, to further consider the effect of surface hydroxyls, the partially hydroxylated γ-Al_2O_3(110) surface is employed to characterize the effect of surface hydroxylation. In this study, we expect to obtain the qualitative effect of γ-Al_2O_3 surface hydroxylation on syngas conversion, not to describe a specific hydroxyl coverage, which could vary under given experimental conditions; thus, only one H_2O molecule is considered for the hydroxylated γ-Al_2O_3(110) surface.

Further, Rh_4 cluster with four Rh atoms is constructed in both tetrahedral (3D) and planar (2D) configurations to model Rh catalyst supported on γ-Al_2O_3(110) surface. Shi et al. [63] have observed that the 2D square planar structure of Rh_4 cluster is less stable than the 3D tetrahedron structure in gas phase, moreover, our results show that upon adsorption on the γ-Al_2O_3(110) surface, Rh_4 cluster with 2D planar structure is also less stable than that with 3D tetrahedron structure. In addition, 3D configuration is the smallest unit to present a three-dimensional structure to probe into metal–metal and metal–support interactions.

Based on above facts, Rh_4 cluster with 3D tetrahedral configuration is adopted to probe into its interaction with γ-Al_2O_3 (110) surface in this study. Thus, when γ-Al_2O_3 surface hydroxyls are considered, two models: Rh_4 cluster with 3D tetrahedral configuration supported on the dry (fully dehydrated) γ-Al_2O_3(110) surface and the partially hydroxylated γ-Al_2O_3(110) surface, have been employed to model Rh/γ-Al_2O_3 catalyst. During all calculations, the bottom two layers of γ-Al_2O_3(110) are fixed, whereas the upper four layers and Rh_4 cluster, as well as the adsorbed species involved in syngas conversion are relaxed.

2.2. Calculation methods

All calculations have been preformed using D mol^3 program in Materials Studio 4.4 package in the framework of DFT [64,65], and the main calculations are based on generalized gradient approximation the (GGA) corrected the exchange-correlation functional proposed by Perdew-Burke-Ernzerhof (PBE) functional. The

double-numerical basis set with a polarization d-function (DNP) is chosen to expand the valence electron functions. The inner electrons of Rh and Al atoms are kept frozen and replaced by an effective core potential (ECP), and other atoms are treated with an all electron basis set. Brillouin-zone integrations have been performed on $2 \times 2 \times 1$ grid Monkhorst-Pack special *k*-points and a Methfessel-Paxton smearing of 0.01 Ha.

In order to determine accurate activation barrier of the reaction, transition states of the reaction are searched by using of complete LST/QST approach [66,67]. Frequency analysis has been used to validate the optimized transition state structures with only one imaginary frequency, and TS confirmation is performed on every transition state to confirm that they lead to the desired reactants and products [68].

The binding energy of Rh_4 cluster with the γ-Al_2O_3 surface (E_{bind}) is calculated as:

$$E_{\text{bind}} = E_{(\gamma-Al_2O_3)} + E_{(Rh_4\text{cluster})} - E_{(Rh_4\text{cluster}/\gamma-Al_2O_3)}$$

where $E_{(\gamma-Al_2O_3)}$, $E_{(Rh_4\text{cluster})}$ and $E_{(Rh_4\text{cluster}/\gamma-Al_2O_3)}$ are the total energy of bare γ-Al_2O_3 surface, isolated Rh_4 cluster, and Rh_4 cluster supported on the γ-Al_2O_3 surface, respectively.

For a reaction such as R (reactant) → P (product) on catalyst surface, the activation barrier (E_a) and reaction energy (ΔE) are calculated according to the following formulas:

$$E_a = E_{TS} - E_R$$

$$\Delta E = E_P - E_R$$

where E_R and E_P are the total energies of the adsorbed reactant and product, respectively, and E_{TS} is the total energy of the transition state.

3. Results and discussion

3.1. Adsorptions of reactants and possible intermediates

The adsorption energy (E_{ads}) is defined as follows:

$$E_{\text{ads}} = [E_{(\text{slab})} + E_{(\text{adsorbate})}] - E_{(\text{adsorbate/slab})}$$

where $E_{(\text{adsorbate/slab})}$, $E_{(\text{slab})}$ and $E_{(\text{adsorbate})}$ are the total energies of the slab with the adsorbate in the equilibrium state, the slab surface and the free adsorbate, respectively. With this definition, more positive values reflect the strong interaction of adsorbed species with Rh/γ-Al_2O_3 catalyst.

The side and top views for the most stable configurations of Rh_4 cluster supported on the dry and the hydroxylated γ-Al_2O_3(110) surfaces have been obtained, which is denoted as D(Rh4) and H(Rh4), respectively, as presented in Fig. 1. Then, the adsorptions of the reactants and all possible intermediates involved in the possible formation pathways of C_2 species have been investigated. By our DFT calculations, the most stable adsorption configurations of these species and the corresponding adsorption energies on D(Rh4) and H(Rh4) surfaces are shown in Figs. 2 and 3, respectively.

3.2. CH_x (x = 1–3) formation from syngas

For CH_x (x = 1–3) formation from syngas, two possibilities exist [69]: one is that CO direct dissociation to produce C + O, followed by C hydrogenation to form CH_x species; the other is that CO hydrogenation to CH_xO or CH_xOH intermediates, followed by the C—O bond cleavage to produce CH_x species. The activation barriers and reaction energies of all possible elementary reactions involved in C_2 species synthesis from syngas on D(Rh4) and H(Rh4) surfaces have been listed in Table 1. Moreover, Figs. 4 and 5 present the summary potential energy diagram for the most favorable formation pathway

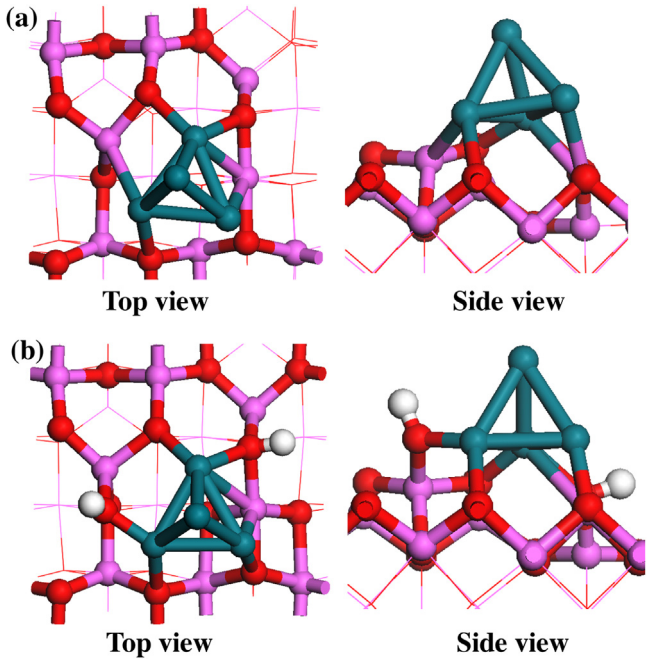

Fig. 1. The top and side views of Rh_4 cluster supported on (a) the dehydrated γ-Al_2O_3(110) surface, D(Rh4), (b) the partially hydrated γ-Al_2O_3(110) surface, H(Rh4). Pink, red, white and dark cyan balls stand for Al, O, H and Rh atoms, respectively. (For interpretation of the references to colour in this figure legend, the reader is referred to the web version of this article.)

Table 1
The possible elementary reactions involved in C_2 species synthesis from syngas on D(Rh4) and H(Rh4) surfaces together with the activation energies (E_a/kJ mol^{-1}) and reaction energies (ΔE/kJ mol^{-1}).

Elementary reactions		D(Rh4)		H(Rh4)	
		E_a	ΔE	E_a	ΔE
(R1)	$CO \rightarrow C + O$	407.0	90.9	400.8	138.5
(R2)	$CO + H \rightarrow CHO$	195.4	85.3	198.5	103.3
(R3)	$CO + H \rightarrow COH$	376.8	170.7	263.8	79.2
(R4)	$CHO \rightarrow CH + O$	135.9	−16.3	187.5	−41.5
(R5)	$CHO + H \rightarrow CHOH$	155.4	48.4	120.4	40.1
(R6)	$CHOH \rightarrow CH + OH$	–	–	141.9	−106.0
(R7)	$CHO + H \rightarrow CH_2O$	125.3	11.0	168.2	13.1
(R8)	$CH_2O \rightarrow CH_2 + O$	94.9	9.9	–	–
(R9)	$CH_2O + H \rightarrow CH_2OH$	206.0	84.8	–	–
(R10)	$CH_2O + H \rightarrow CH_3O$	110.5	−16.2	–	–
(R11)	$CHOH + H \rightarrow CH_2OH$	–	–	143.4	46.6
(R12)	$CH_2OH \rightarrow CH_2 + OH$	–	–	98.8	−86.7
(R13)	$CH_2OH + H \rightarrow CH_3OH$	–	–	137.5	25.0
(R14)	$CH_3O \rightarrow CH_3 + O$	211.3	51.2	–	–
(R15)	$CH_3O + H \rightarrow CH_3OH$	204.2	76.8	–	–
(R16)	$CH + CO \rightarrow CHCO$	164.9	63.5	121.7	74.2
(R17)	$CH + CHO \rightarrow CHCHO$	134.9	7.0	162.0	−27.0
(R18)	$CH + H \rightarrow CH_2$	108.5	17.7	167.5	32.3
(R19)	$CH \rightarrow C + H$	130.0	29.1	156.3	21.5
(R20)	$CH + CH \rightarrow C_2H_2$	37.4	−27.7	106.1	−24.0
(R21)	$CH_2 + CO \rightarrow CH_2CO$	294.9	20.5	132.8	65.0
(R22)	$CH_2 + CHO \rightarrow CH_2CHO$	296.4	18.7	95.8	31.4
(R23)	$CH_2 + H \rightarrow CH_3$	146.0	33.2	94.8	26.3
(R24)	$CH_2 \rightarrow CH + H$	90.8	−17.7	135.3	−32.3
(R25)	$CH_2 + CH_2 \rightarrow C_2H_4$	199.2	−13.8	166.8	2.3
(R26)	$CH_3 + CO \rightarrow CH_3CO$	–	–	188.6	84.2
(R27)	$CH_3 + CHO \rightarrow CH_3CHO$	–	–	123.3	26.3
(R28)	$CH_3 + H \rightarrow CH_4$	–	–	76.3	18.7
(R29)	$CH_3 \rightarrow CH_2 + H$	–	–	68.5	−26.3
(R30)	$CH_3 + CH_3 \rightarrow C_2H_6$	–	–	184.6	17.8

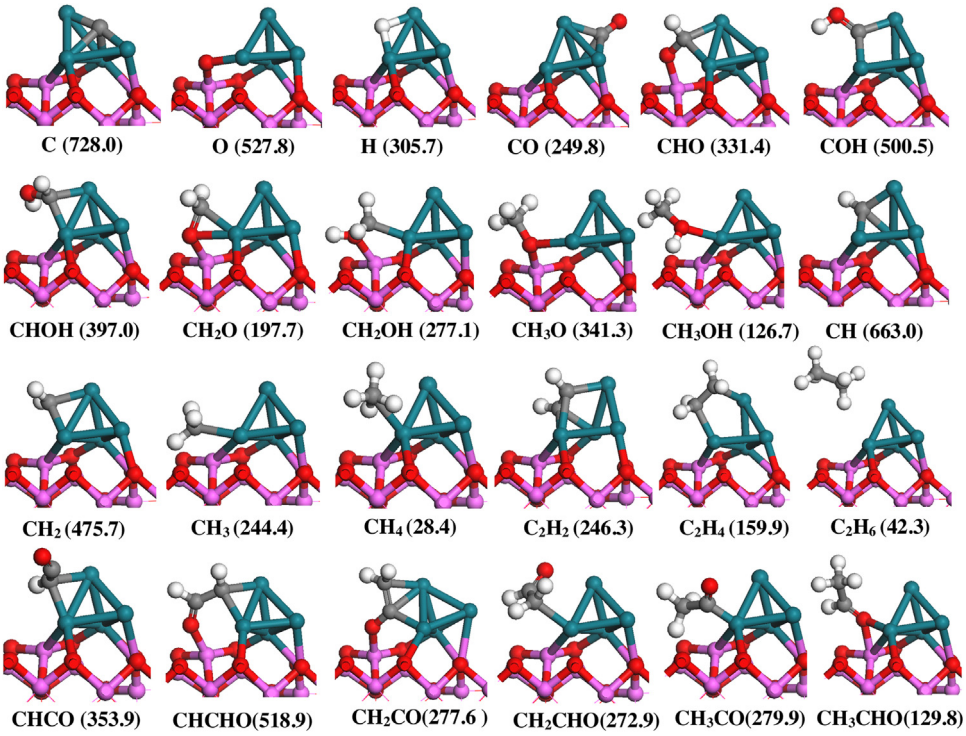

Fig. 2. The most stable adsorption configurations and the corresponding adsorption energies of all possible species involved in the possible formation pathways of C_2 species on D(Rh4). C, O, H, Al and Rh atoms are shown in the grey, red, white, light pink and dark cyan balls, respectively. The data in the parenthesis are the adsorption energies (in kJ mol^{-1}). (For interpretation of the references to colour in this figure legend, the reader is referred to the web version of this article.)

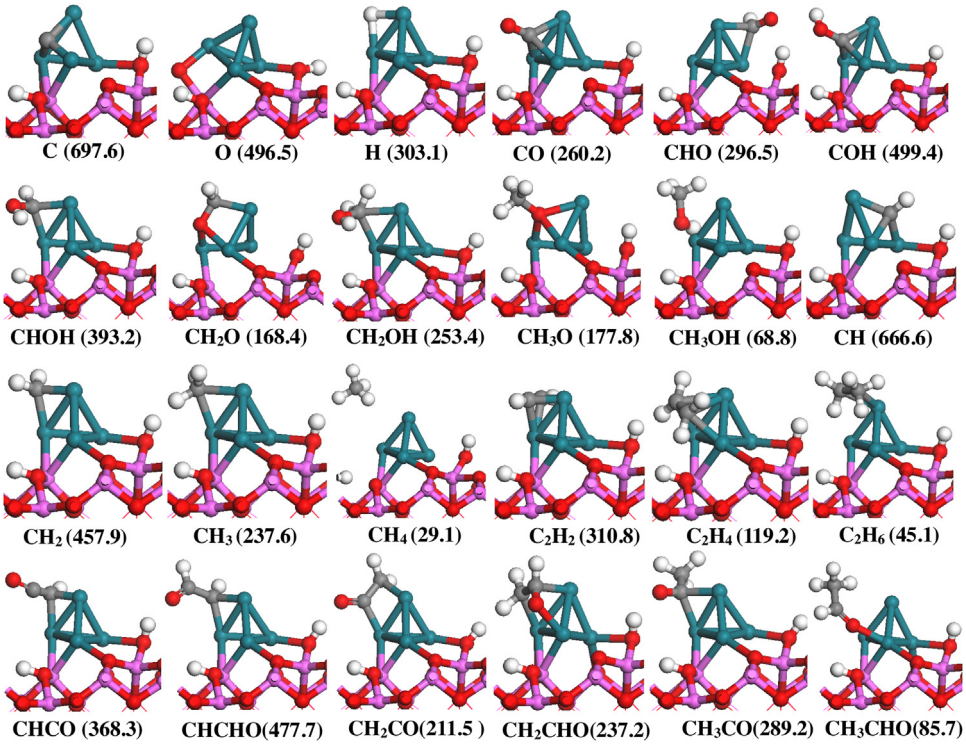

Fig. 3. The most stable adsorption configurations and the corresponding adsorption energies of all possible species involved in the possible formation pathways of C_2 species on H(Rh4). See Fig. 2 for color coding. The data in the parenthesis are the adsorption energies (in kJ mol^{-1}).

of CH_x (x = 1–3) and CH_3OH species together with the structures of initial states (ISs), transition states (TSs) and final states (FSs) on D(Rh4) and H(Rh4) surfaces, respectively.

3.2.1. CO dissociation and hydrogenation

Three Reactions (R1–R3) may occur for CO initial step. The detailed potential energy profile of these reactions together with

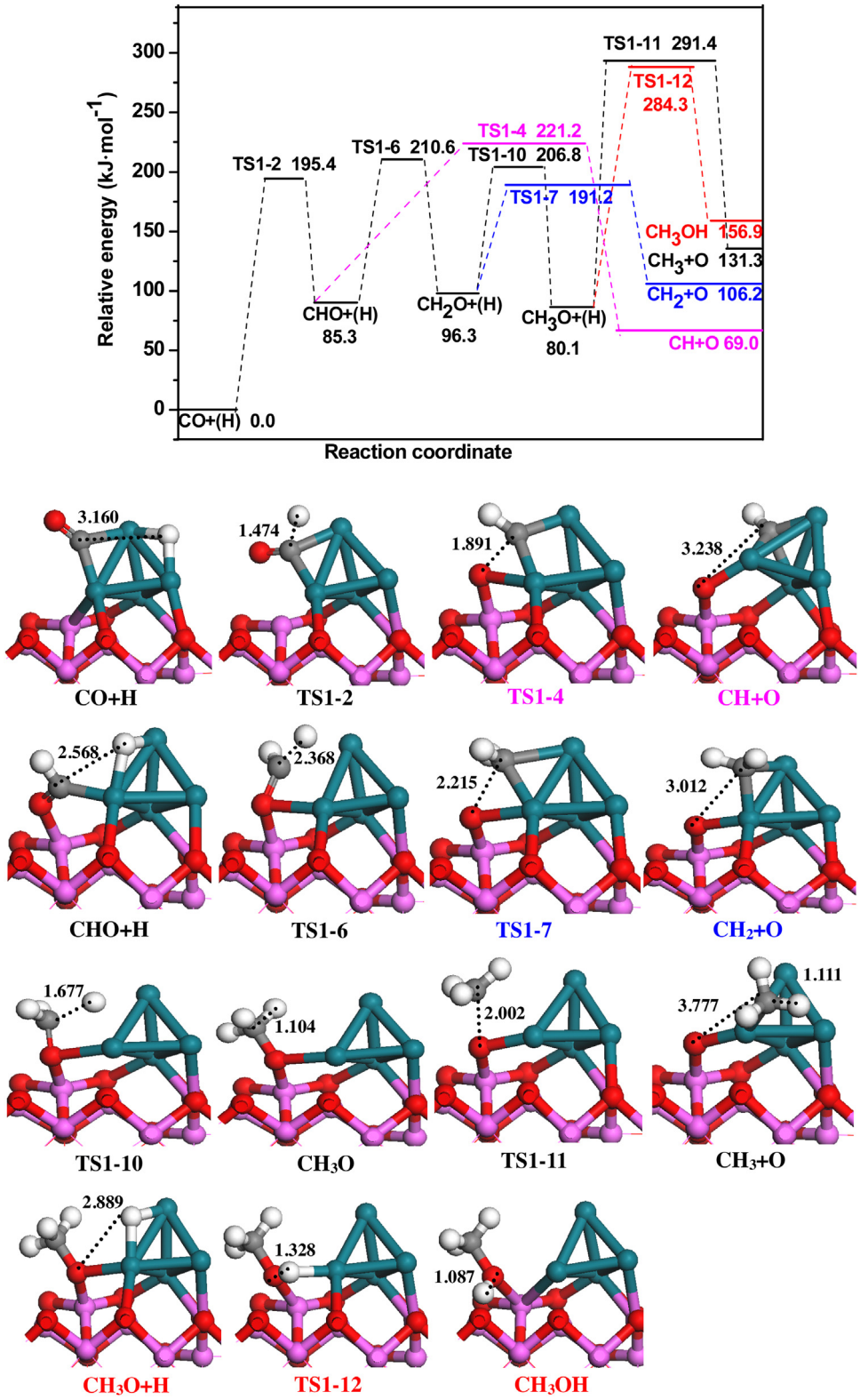

Fig. 4. The potential energy diagram of the most favorable route for the formation of CH_x (x = 1–3) species and CH_3OH together with ISs, TSs and FSs on D(Rh4). Bond lengths are in Å. See Fig. 2 for color coding.

the ISs, TSs and FSs on D(Rh4) and H(Rh4) surfaces are displayed in Figs. S1 and S2 in the Supporting information, respectively.

Our results show that when CO and H is co-adsorbed on D(Rh4) and H(Rh4) surfaces, respectively, CO direct dissociation is not energetically favored; CO is dominantly hydrogenated to form CHO, which is much more favorable kinetically than COH formation and CO direct dissociation, indicating that CHO is the major product of CO initial step. Thus, the subsequent formations of CH_x, CH_xO and CH_xOH species can only start with CHO.

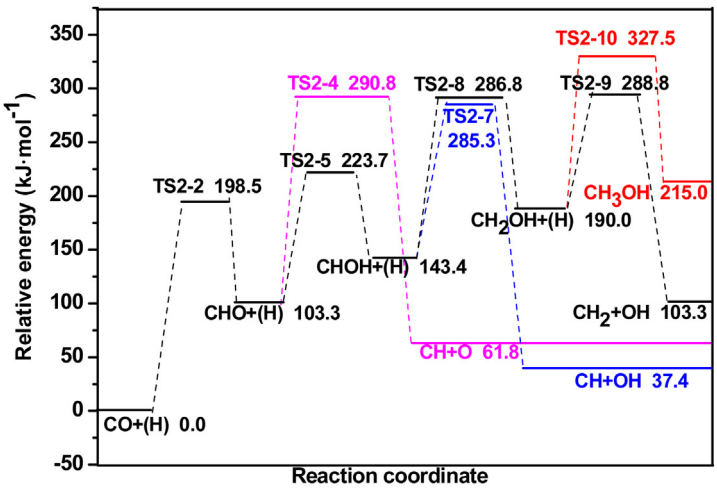

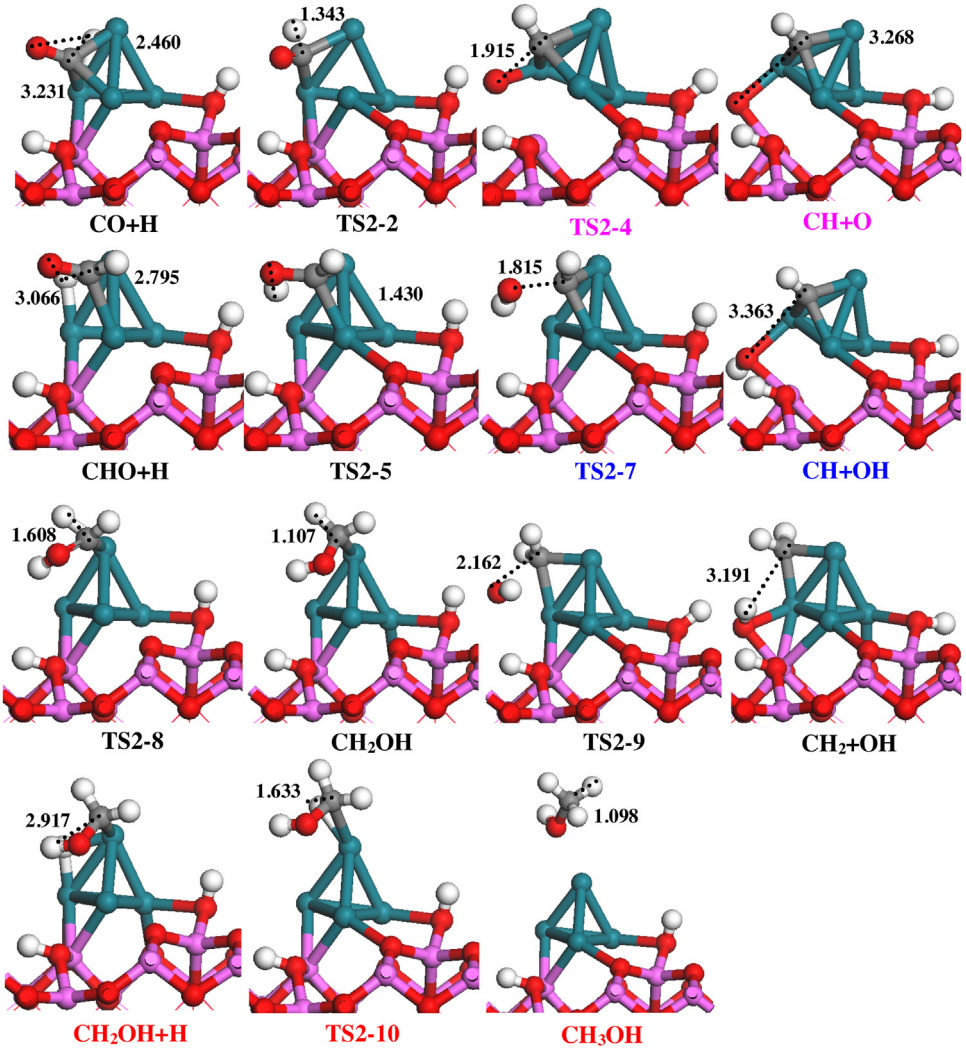

Fig. 5. The potential energy diagram of the most favorable route for the formation of CH_x(x = 1,2) species and CH_3OH together with ISs, TSs and FSs on H(Rh4). Bond lengths are in Å. See Fig. 2 for color coding.

3.2.2. *CH formation*

As mentioned above, CHO is the dominant product for CO hydrogenation on D(Rh4) and H(Rh4), as a result, CH formation is considered only by CHO and CHO + H in this study, one is the direct C—O bond dissociation of CHO to CH + O (R4); the other is CHO hydrogenation to CHOH, followed by the C—O bond cleavage to CH (R5, R6). Meanwhile, CHO hydrogenation to CH_2O (R7) is also considered. The detailed potential energy profiles of these reactions together with the corresponding structures on D(Rh4) and H(Rh4)

surfaces are shown in Figs. S3 and S4 in the Supporting information, respectively.

3.2.2.1. On D(Rh4) surface. As shown in Fig. 4, our results show that CH is dominantly formed by the direct C—O bond scission of CHO, $CHO \rightarrow CH + O$, which has the relatively lower activation barrier of 135.9 kJ mol^{-1}. Meanwhile, the reaction of $CHO + H \rightarrow CH_2O$ has the activation barrier of 125.3 kJ mol^{-1}, which reveals that with respect to CO + H species, the formations of CH and CH_2O are two parallel reactions in kinetics with the corresponding highest barriers of 221.2 and 210.6 kJ mol^{-1}, respectively. Moreover, CHO hydrogenation to CH_2O (R7) with the activation barrier of 125.3 kJ mol^{-1} is more favorable than CHO hydrogenation to CHOH (R5) with the activation barrier of 155.4 kJ mol^{-1}; thus, starting from CHO species, CH and CH_2O are the dominant products on D(Rh4) surface.

3.2.2.2. On H(Rh4) surface. As shown in Fig. 5, for CH formation, $CO + H \rightarrow CHO + H \rightarrow CHOH \rightarrow CH + OH$ and $CO + H \rightarrow CHO \rightarrow CH + O$ are two parallel reactions in kinetics, with respect to CO + H species, the corresponding highest barriers are 285.3 and 290.8 kJ mol^{-1}, respectively. However, CHO hydrogenation to CHOH (R5) with the activation barrier of 120.4 kJ mol^{-1} is more favorable than CHO hydrogenation to CH_2O (R7) with the activation barrier of 168.2 kJ mol^{-1}; namely, for CHO hydrogenation, CHO prefers to be hydrogenated to CHOH rather than being hydrogenated to CH_2O formation on H(Rh4) surface, which is quite different from D(Rh4) surface. Therefore, starting from CHO species, CH and CHOH are the dominant products on H(Rh4) surface.

3.2.3. CH_2 formation

There are two possibilities for CH_2 formation, one is the direct C—O bond dissociation of CH_2O (R8), and the other is the direct C—O bond dissociation of CH_2OH (R12). As mentioned above, CHO prefers to be hydrogenated to CH_2O on D(Rh4) surface, while CHO prefers to be hydrogenated to CHOH on H(Rh4) surface; thus, starting from CH_2O and CHOH species (R9–R11) on D(Rh4) and H(Rh4) surfaces, respectively, the detailed potential energy profiles of CH_2 formation together with the corresponding structures on D(Rh4) and H(Rh4) surfaces are shown in Figs. S5 and S6 in the Supporting information, respectively.

3.2.3.1. On D(Rh4) surface. As shown in Fig. 4, with respect to CO + H species, $CO + H \rightarrow CHO + H \rightarrow CH_2O \rightarrow CH_2 + O$ (R2, R7, R8) is the most favorable pathway of CH_2 formation in kinetics. Meanwhile, CH_2O hydrogenation to CH_3O (R10) can compete with CH_2O direct dissociation (R8); moreover, both pathways have the same highest barrier of 210.6 kJ mol^{-1}. Therefore, $CO + H \rightarrow CHO + H \rightarrow CH_2O \rightarrow CH_2 + O$ and $CO + H \rightarrow CHO + H \rightarrow CH_2O + H \rightarrow CH_3O$ are two parallel pathways, namely, CH_2 and CH_3O are the dominant products on D(Rh4) surface.

3.2.3.2. On H(Rh4) surface. As shown in Fig. 5, with respect to CO + H species, $CO + H \rightarrow CHO + H \rightarrow CHOH + H \rightarrow CH_2OH \rightarrow CH_2 + OH$ is the most favorable pathway of CH_2 formation in kinetics, which has the highest barrier of 288.8 kJ mol^{-1}. Meanwhile, CH_3OH formation by CH_2OH hydrogenation (R13) ($CO + H \rightarrow CHO + H \rightarrow CHOH + H \rightarrow CH_2OH + H \rightarrow CH_3OH$) has the highest barrier of 327.5 kJ mol^{-1}, indicating that CH_2OH prefers to be dissociated into CH_2 rather than being hydrogenated to CH_3OH on H(Rh4) surface.

3.2.4. CH_3 formation

According to above results, on D(Rh4) surface, CH_2 and CH_3O are the dominant products; however, on H(Rh4) surface, CH_2 is the dominant product; thus, only on D(Rh4) surface, the direct C—O bond scission of CH_3O can form CH_3 (R14). In addition, CH_3O hydrogenation to CH_3OH (R15) is also examined.

As shown in Fig. 4, with respect to CO + H species, the pathway of $CO + H \rightarrow CHO + H \rightarrow CH_2O + H \rightarrow CH_3O \rightarrow CH_3 + O$ is dominantly responsible for CH_3 formation with the highest barrier of 291.4 kJ mol^{-1}, which competes with CH_3O hydrogenation to CH_3OH with the highest barrier of 284.3 kJ mol^{-1}, indicating that starting from CH_3O species, CH_3 and CH_3OH are the dominant products on D(Rh4) surface.

3.2.5. The most favorable CH_x (x = 1–3) monomer and CH_3OH formations

With respect to CO + H species, on D(Rh4) surface, as shown in Fig. 4, CH is formed via the pathway of $CO + H \rightarrow CHO \rightarrow CH + O$ with the highest barrier and reaction energy of 222.1 and 69.0 kJ mol^{-1}, respectively; CH_2 is formed via the pathway of $CO + H \rightarrow CHO + H \rightarrow CH_2O \rightarrow CH_2 + O$ with the highest barrier and reaction energy of 210.6 and 106.2 kJ mol^{-1}, respectively; CH_3 is formed via the pathway of $CO + H \rightarrow CHO + H \rightarrow CH_2O + H \rightarrow CH_3O \rightarrow CH_3 + O$ with the highest barrier and reaction energy of 291.4 and 131.3 kJ mol^{-1}; CH_3OH is formed via the pathway of $CO + H \rightarrow CHO + H \rightarrow CH_2O + H \rightarrow CH_3O + H \rightarrow CH_3OH$ with the highest barrier and reaction energy of 284.3 and 156.9 kJ mol^{-1}. As a result, we can conclude that CH and CH_2 formations are much more easier than CH_3 and CH_3OH formations, indicating that CH and CH_2 are the most favorable monomer among all CH_x (x = 1-3) species rather than CH_3 and CH_3OH on D(Rh4) surface.

Similarly, from Fig. 5, it can be also found that CH and CH_2 formations ($CO + H \rightarrow CHO + H \rightarrow CHOH \rightarrow CH + OH/CHO \rightarrow CH + O$ and $CO + H \rightarrow CHO + H \rightarrow CHOH + H \rightarrow CH_2OH \rightarrow CH_2 + OH$) have the highest barriers of 290.8/285.3 and 288.8 kJ mol^{-1} on H(Rh4) surface, respectively, which are favorable than CH_3OH formation ($CO + H \rightarrow CHO + H \rightarrow CHOH + H \rightarrow CH_2OH + H \rightarrow CH_3OH$) with the highest barrier of 327.5 kJ mol^{-1}, suggesting that indicating that CH and CH_2 are the most favorable monomer among all CH_x (x = 1–3) species rather than CH_3OH on H(Rh4) surface.

On the basis of above results, we can conclude that Rh/Al_2O_3 catalyst (D(Rh4) and H(Rh4)) can exhibit the relative higher selectivity towards CH and CH_2 formations rather than CH_3 and CH_3OH in syngas conversion; since CH_x is proposed to be a prerequisite for C—C chain formation from syngas, more CH_x is beneficial to produce C_2 species [49,69,70]; therefore, Rh/Al_2O_3 catalyst can provide abundant CH and CH_2 species to participate into the formation of C_2 species.

3.3. C—C chain formation

For C—C chain formation, previous studies by Zhao et al. [50] have found that CHO insertion into CH_x(x = 1–3) is superior and/or competitive to CO insertion and carbene coupling on Rh(111) and Co(0001) surface; moreover, the reports by Kapur et al. [71] have shown that CH_2 is the precursor for C—C chain formation on Rh(111) and Rh(211) surfaces. Thus, since CH and CH_2 are the most favored monomer among all CH_x(x = 1-3) species on D(Rh4) and H(Rh4) surfaces, in this section, we further investigate CO/CHO insertion into CH_x(x = 1,2) to C_2 oxygenates and CH_x coupling to C_2 hydrocarbons, as well as CH_x dissociation and hydrogenation on D(Rh4) and H(Rh4) surfaces. The detailed potential energy profiles for these reactions on D(Rh4) and H(Rh4) surfaces together with the corresponding structures are presented in Figs. S8–S12 in the Supporting information. Meanwhile, Fig. 6 presents the potential energy profile for the most favorable pathways of C—C chain on D(Rh4) and H(Rh4) surfaces.

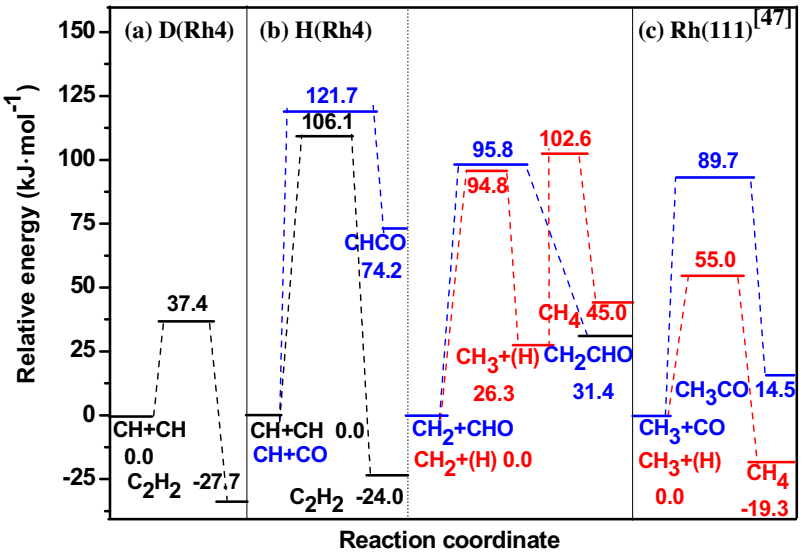

Fig. 6. The potential energy profile comparisons for the most favorable pathways of C_2 species and CH_4 formations on (a) D(Rh4), (b) H(Rh4) and (c) Rh(111) surfaces.

3.3.1. D(Rh4) surface

Our results show that CH coupling, CH + CH → C_2H_2, is the most favorable both thermodynamically and dynamically with the activation barrier and reaction energy of 37.4 and −27.7 kJ mol^{-1} among all reactions related to CH species (R16–R20). On the other hand, among all reactions related to CH_2 species (R21–R25), CH_2 species prefers to be dissociated into CH species (CH_2 → CH + H) both thermodynamically and dynamically with the activation barrier and reaction energy of 90.8 and −17.7 kJ mol^{-1} rather than other reactions, subsequently, CH coupling leads to C_2H_2 formation; Overall, among all reactions related to CH_x(x = 1,2), C_2 hydrocarbon (C_2H_2) is the dominant product on D(Rh4) surface.

3.3.2. H(Rh4) surface

Firstly, among all reactions related to CH species, CH coupling, CH + CH → C_2H_2, is still the most favorable both thermodynamically and dynamically with the activation barrier and reaction energy of 106.1 and −24.0 kJ mol^{-1}, respectively; then, the reaction of CH + CO → CHCO (R16) has the activation barrier and reaction energy of 121.7 and 74.2 kJ mol^{-1}, respectively.

Among all reactions related to CH_2 species, CHO insertion into CH_2 to CH_2CHO competes with CH_2 hydrogenation to CH_3 (95.8 vs. 94.8 kJ mol^{-1}), subsequently, we further investigate all reactions related to CH_3 (R26–R30), suggesting that CH_3 dissociation or hydrogenation to CH_2 or CH_4 (68.5 vs. 76.3 kJ mol^{-1}) is more favorable than other reactions, namely, once CH_3 species is formed, partial CH_3 can be hydrogenated to form CH_4, the other can be dissociation into CH_2, which continues to participate into the formations of C_2 oxygenates (CH_2CHO) and CH_3.

As illustrated in Fig. 6(b), we can obtain that on H(Rh4) surface, CH species is responsible for the formations of C_2 oxygenate (CHCO) and C_2 hydrocarbon (C_2H_2); CH_2 species mainly contribute to the formations of C_2 oxygenate (CH_2CHO) and methane (CH_4). Namely, C_2 oxygenates and hydrocarbon are the dominant products, meanwhile, CH_4 formation can compete with C_2 species, which are in consistent with the experimental results [27,69].

3.4. General discussion

3.4.1. Selectivity between CH_x and CH_3OH on D(Rh4), H(Rh4) and Rh(111)

As mentioned above, CHO species is the major product of CO initial step on D(Rh4) and H(Rh4) surfaces, which is agreement with the previous studies on Rh(111) surface [49]. Moreover, CH and CH_2 species are the dominant existence form of CH_x (x = 1-3) rather than CH_3 and CH_3OH on D(Rh4) and H(Rh4); while CH_3 species is the dominant existence form of CH_x (x = 1–3) on the pure Rh(111) surface rather than CH_3OH.

Interestingly, to better understand the effect of γ-Al_2O_3 support and its surface properties on reaction behavior of syngas conversion compared to the pure Rh(111) surfaces, it is necessary to quantify the selectivity between CH_x and CH_3OH on Rh-supported on γ-Al_2O_3 surface (D(Rh4), H(Rh4)) and the pure Rh(111) surface, the effective barrier difference between CH_x and CH_3OH formations is used a descriptor. In principle, the higher barrier difference represents the higher selectivity of CH_x and the lower selectivity of CH_3OH. Starting from CHO species, Fig. 7 presents the comparisons for the potential energy profile of the most favorable CH_x(x = 1–3) and methanol formations on D(Rh4), H(Rh4) and Rh(111) surfaces.

As shown in Fig. 7, with respect to CHO or CHO + H species, our calculated energy differences of the highest barrier between CH_x and CH_3OH formations are 73.7 and 63.1 kJ mol^{-1} on D(Rh4) surface, 36.7 and 38.7 kJ mol^{-1} on H(Rh4) surface, as well as −25.1 kJ mol^{-1} on Rh(111) surfaces, respectively; obviously, D(Rh4) and H(Rh4) surfaces exhibit the higher selectivity of CH_x (x = 1,2), as well as the lower selectivity of CH_3OH, moreover, D(Rh4) is more favorable than H(Rh4) surfaces for CH_x (x = 1,2) selectivity due to the different surface properties, which implies that CH_3OH formation can not compete with CH_x (x = 1,2) in syngas conversion on D(Rh4) and H(Rh4) surfaces. Whereas, the pure Rh(111) surface exhibits the higher selectivity of CH_3OH and the lower selectivity of CH_3.

Above results suggest that compared to the pure Rh(111) surface, the catalytic selectivity of Rh catalyst toward CH_x (x = 1–3) formation obviously depends on γ-Al_2O_3 support and its surface properties; Rh-supported on γ-Al_2O_3 can change the dominant existence form of CH_x (x = 1–3) species, provide the abundant CH_x (x = 1,2) source to participate into the formation of C_2 species, and inhibit methanol formation.

3.4.2. Selectivity of C_2 species on D(Rh4), H(Rh4) and Rh(111)

Fig. 6 presents the potential energy profile comparison for the most favorable pathways of C_2 species and CH_4 formation on D(Rh4), H(Rh4) and Rh(111) surfaces. On D(Rh4) surface, CH species coupling to form C_2H_2 is dominantly responsible for the forma-

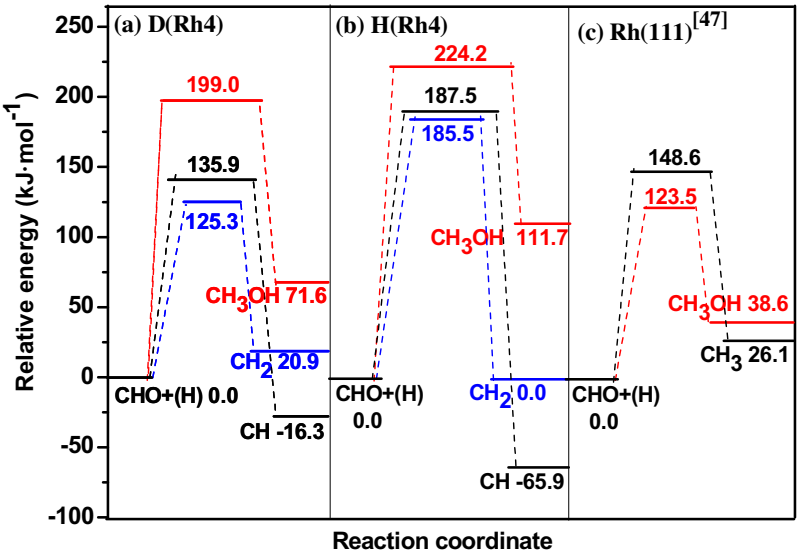

Fig. 7. The comparisons for the potential energy profile of the most favorable CH_x(x = 1–3) and CH_3OH formations on (a) D(Rh4), (b) H(Rh4) and (c) Rh(111) surfaces.

tions of C_2 species. On H(Rh4) surface, starting from CH species, CH coupling to C_2H_2 is competitive with CHCO formation by CO insertion into CH (106.1 vs. 121.7 kJ mol^{-1}); starting from CH_2 species, CHO insertion into CH_2 to CH_2CHO competes with CH_4 formation by CH_2 successive hydrogenation (95.8 vs. 102.6 kJ mol^{-1}); thus, C_2 oxygenates ($CHCO$,CH_2CHO), C_2 hydrocarbon (C_2H_2) and CH_4 are the main products starting from CH_x(x = 1,2) on H(Rh4) surface. However, on the pure Rh(111) surface [49], CH_3 prefers to be hydrogenated to CH_4 rather than being formed C_2 oxygenates by CO insertion into CH_3 (55.0 vs. 89.7 kJ mol^{-1}), namely, the pure Rh(111) surface is more favorable for CH_4 formation rather than C_2 species. As a result, compared to the pure Rh(111) surface, Rh_4 cluster supported on γ-Al_2O_3(110) surface (D(Rh4) and H(Rh4)) not only promote the productivity and selectivity of C_2 species, but also suppress CH_4 formation to some extent.

On the other hand, by comparing the selectivity of C_2 species between D(Rh4) and H(Rh4) surfaces, we can obtain that D(Rh4) with Rh_4 cluster supported on the dry γ-Al_2O_3(110) surface is more favorable to form C_2 hydrocarbons (C_2H_2), whereas, H(Rh4) with Rh_4 cluster supported on the hydroxylated γ-Al_2O_3(110) surface not only produces C_2 hydrocarbons (C_2H_2), but also easily forms C_2 oxygenates ($CHCO$,CH_2CHO), indicating that the surface hydroxyls of γ-Al_2O_3 support can affect the selectivity of C_2 species over Rh/γ-Al_2O_3 catalyst in syngas conversion.

Therefore, when Rh-based catalysts are developed for C_2 species synthesis from syngas, the catalytic activities of the catalysts toward CH_x formation and C—C bond formation have to be especially considered. This is the reason why to achieve high C_2 species productivity and selectivity, promoters and/or supports have to be employed for Rh catalysts to tune the reactivity and selectivity of key steps in syngas conversion, which should minimize CH_3OH and CH_4 production and/or maximize CH_x formation and chain growth from C_1 species to C_2 species. In addition, extensive studies about the effect of promoters added into Rh/γ-Al_2O_3 catalyst on the catalytic performance of syngas conversion to C_2 species will be carried out in our next work, which is beyond the scope of present studies.

4. Conclusions

In the present study, density functional theory method together with periodic slab model have been employed to probe into a comparative study of the preference formation mechanisms of CH_x (x = 1-3) and C_2 species in syngas conversion on Rh_4 cluster supported on the dry and hydroxylated γ-Al_2O_3(110) surfaces, denoted as D(Rh4) and H(Rh4), respectively. Meanwhile, compare to the pure Rh(111) surface, the effect of γ-Al_2O_3 support and its surface properties on reaction behavior of syngas conversion has been identified. Our results show that CHO is the dominant product for CO initial step. Then, starting from CHO, CH and CH_2 species are dominantly formed rather than CH_3 and CH_3OH on D(Rh4) and H(Rh4), namely, compared to the pure Rh(111) surface, Rh cluster supported on γ-Al_2O_3 can exhibit high selectivity for CH_x formation. On the other hand, the hydrogenation, dissociation and coupling of CH_x(x = 1,2), as well as CO/CHO insertion into CH_x(x = 1,2) show that D(Rh4) surface is more easier to C_2 hydrocarbon (C_2H_2) formation, whereas, H(Rh4) surface easily produces C_2 hydrocarbon (C_2H_2) and oxygenates ($CHCO$,CH_2CHO), which compete with CH_4 formation, indicating that the surface hydroxyls of support γ-Al_2O_3 can affect the selectivity of C_2 species over Rh/γ-Al_2O_3 catalyst in syngas conversion; meanwhile, compared to the pure Rh(111) surface with CH_4 formation rather than C_2 species formation, Rh/γ-Al_2O_3 catalyst can promote C_2 species formation.

Acknowledgments

This work is financially supported by the National Natural Science Foundation of China (Nos. 21276003, 21476155 and 21276171), the Natural Science Foundation of Shanxi Province (No. 2014011012-2), the Program for the Top Young Academic Leaders of Higher Learning Institutions of Shanxi, and the Top Young Innovative Talents of Shanxi.

Appendix A. Supplementary data

Supplementary data associated with this article can be found, in the online version, at http://dx.doi.org/10.1016/j.apsusc.2016.04.106.

References

[1] X. Pan, Z. Fan, W. Chen, Y. Ding, H. Luo, X. Bao, Enhanced ethanol production inside carbon-nanotube reactors containing catalytic particles, Nat. Mater. 6 (2007) 507–511.

[2] Y.H. Zhao, M.M. Yang, D. Sun, H.Y. Su, K. Sun, X. Ma, X. Bao, W.X. Li, Rh-decorated Cu alloy catalyst for improved C_2 oxygenate formation from syngas, J. Phys. Chem. C 115 (2011) 18247–18256.
[3] H. Yin, Y. Ding, H. Luo, H. Zhu, D. He, J. Xiong, L. Lin, Influence of iron promoter on catalytic properties of Rh-Mn-Li/SiO_2 for CO hydrogenation, Appl. Catal. A: Gen. 243 (2003) 155–164.
[4] M.A. Haider, M.R. Gogate, R.J. Davis, Fe-promotion of supported Rh catalysts for direct conversion of syngas to ethanol, J. Catal. 261 (2009) 9–16.
[5] G.R. Jenness, J. Schmidt, Unraveling the role of metal–support interactions in heterogeneous catalysis: oxygenate selectivity in Fischer–Tropsch synthesis, ACS Catal. 3 (2013) 2881–2890.
[6] K. Fang, D. Li, M. Lin, M. Xiang, W. Wei, Y. Sun, A short review of heterogeneous catalytic process for mixed alcohols synthesis via syngas, Catal. Today 147 (2009) 133–138.
[7] F. Li, D.E. Jiang, X.C. Zeng, Z. Chen, Mn monolayer modified Rh for syngas-to-ethanol conversion: a first-principles study, Nanoscale 4 (2012) 1123–1129.
[8] D. Mei, R. Rousseau, S.M. Kathmann, V.A. Glezakou, M.H. Engelhard, W. Jiang, C. Wang, M.A. Gerber, J.F. White, D.J. Stevens, Ethanol synthesis from syngas over Rh-based/SiO_2 catalysts: a combined experimental and theoretical modeling study, J. Catal. 271 (2010) 325–342.
[9] H. Arakawa, T. Fukushima, M. Ichikawa, S. Natsushita, K. Takeuchi, T. Matsuzaki, Y. Sugi, Selective synthesis of ethanol over Rh–Ti–Fe–Ir/SiO_2 catalyst at high pressure syngas conversion, Catal. Lett. 14 (1985) 881–884.
[10] V.A. Glezakou, J.E. Jaffe, R. Rousseau, D. Mei, S.M. Kathmann, K.O. Albrecht, M.J. Gray, M.A. Gerber, The role of Ir in ternary Rh-based catalysts for syngas conversion to C_2^+ oxygenates, Top. Catal. 55 (2012) 595–600.
[11] H. Luo, W. Zhang, H. Zhou, S. Huang, P. Lin, Y. Ding, L. Lin, A study of Rh-Sm-V/SiO_2 catalysts for the preparation of C_2-oxygenates from syngas, Appl. Catal. A: Gen. 214 (2001) 161–166.
[12] H.M. Yin, Y.J. Ding, H.Y. Luo, D.P. He, W.M. Chen, Z.Y. Ao, L.W. Lin, A kinetic study of selective hydrogenation of carbon monoxide to C_2 oxygenates on Rh-Mn-Li-Fe/SiO_2 catalyst, J. Energ. Chem. 12 (2003) 233–236.
[13] M. Ichikawa, T. Fukushima, Mechanism of syngas conversion into C_2-oxygenates such as ethanol catalysed on a SiO_2-supported Rh–Ti catalyst, J. Chem. Soc. Chem. Commun. (1985) 321–323.
[14] L. Han, D. Mao, J. Yu, Q. Guo, G. Lu, Synthesis of C_2-oxygenates from syngas over Rh-based catalyst supported on SiO_2, TiO_2 and SiO_2–TiO_2 mixed oxide, Catal. Commun. 23 (2012) 20–24.
[15] X. Mo, J. Gao, N. Umnajkaseam, J.G. Goodwin, La, V, and Fe promotion of Rh/SiO_2 for CO hydrogenation: effect on adsorption and reaction, J. Catal. 267 (2009) 167–176.
[16] J. Gao, X. Mo, A.C.Y. Chien, W. Torres, J.G. Goodwin, CO hydrogenation on lanthana and vanadia doubly promoted Rh/SiO_2 catalysts, J. Catal. 262 (2009) 119–126.
[17] R. Burch, M.I. Petch, Investigation of the synthesis of oxygenates from carbon monoxide/hydrogen mixtures on supported rhodium catalysts, Appl. Catal. A: Gen. 88 (1992) 39–60.
[18] A. Egbebi, V. Schwartz, S.H. Overbury, J.J. Spivey, Effect of Li promoter on titania- supported Rh catalyst for ethanol formation from CO hydrogenation, Catal. Today 149 (2010) 91–97.
[19] H. Ngo, Y. Liu, K. Murata, Effect of secondary additives (Li, Mn) in Fe-Promoted Rh/TiO_2 catalysts for the synthesis of ethanol from syngas, React. Kinet. Mech. Cat. 102 (2011) 425–435.
[20] R.P. Underwood, A.T. Bell, Influence of particle size on carbon monoxide hydrogenation over silica-and lanthana-supported rhodium, Appl. Catal. 34 (1987) 289–310.
[21] M. Ichikawa, Catalysis by supported metal crystallites from carbonyl clusters. II. catalytic ethanol synthesis from CO and H_2 under atmospheric pressure over supported rhodium crystallites prepared from Rh carbonyl clusters deposited on TiO_2, ZrO_2, and La_2O_3, Bull. Chem. Soc. Jpn. 51 (1978) 2273–2277.
[22] P. Gajardo, E. Gleason, J. Katzer, A. Sleight, Preparation and characterization of highly dispersed rhodium on Al_2O_2, TiO_2 ZrO_2, and CeO_2, Stud. Surf. Sci. Catal. 7 (1981) 1462–1463.
[23] J.R. Katzer, A.W. Sleight, P. Gajardo, J.B. Michel, E.F. Gleason, S. McMillan, The role of the support in CO hydrogenation selectivity of supported rhodium, Faraday Discuss. Chem. Soc. 72 (1981) 121–133.
[24] P. Gronchi, E. Tempesti, C. Mazzocchia, Metal dispersion dependent selectivities for syngas conversion to ethanol on V_2O_3 supported rhodium, Appl. Catal. A: Gen. 120 (1994) 115–126.
[25] R. Burch, M. Hayes, The preparation and characterisation of Fe-promoted Al_2O_3-supported Rh catalysts for the selective production of ethanol from syngas, J. Catal. 165 (1997) 249–261.
[26] M. Ojeda, M.L. Granados, S. Rojas, P. Terreros, F.J. García-García, J.L.G. Fierro, Manganese-promoted Rh/Al_2O_3 for C_2-oxygenates synthesis from syngas: effect of manganese loading, Appl. Catal. A: Gen. 261 (2004) 47–55.
[27] X.D. Xu, E. Doesburg, J. Scholten, Synthesis of higher alcohols from syngas-recently patented catalysts and tentative ideas on the mechanism, Catal. Today 2 (1987) 125–170.
[28] I. Wachs, G. Deo, D. Kim, M. Vuurman, H. Hu, Molecular design of supported metal oxide catalysts, Stud. Surf. Sci. Catal. 75 (1993) 543–557.
[29] M. Cabero, M. Holgado, V. Rives, Effect of doping agents and of crystallographic phase on the adsorption properties of titania-supported rhodium, Mater. Chem. Phys. 27 (1991) 181–188.
[30] I.E. Wachs, G. Deo, M.A. Vuurman, H. Hu, J.M. Jehng, Molecular design of supported metal oxide catalysts: an initial step to theoretical models, J. Mol. Catal. 82 (1993) 443–455.
[31] U. Usman, M. Takaki, T. Kubota, Y. Okamoto, Effect of boron addition on a MoO_3/Al_2O_3 catalyst: physicochemical characterization, Appl. Catal. A: Gen. 286 (2005) 148–154.
[32] Z.J. Zuo, L. Wang, P.D. Han, W. Huang, Methanol synthesis by CO and CO_2 hydrogenation on Cu/γ-Al_2O_3 surface in liquid paraffin solution, Appl. Surf. Sci. 290 (2014) 398–404.
[33] J.H. Flores, D.P.B. Peixoto, L.G. Appel, R.R. de Avillez, M.I. Pais da Silva, The influence of different methanol synthesis catalysts on direct synthesis of DME from syngas, Catal. Today 172 (2011) 218–225.
[34] X.B. Zhang, Z. Li, Q.H. Guo, H. Fan, H.Y. Zheng, K.C. Xie, Influence of the calcination on the activity and stability of the Cu/ZnO/Al_2O_3 catalyst in liquid phase methanol synthesis, Fuel 89 (2010) 1348–1352.
[35] D.G. Cheng, X.L. Zhu, Y.H. Ben, F. He, L. Cui, C.J. Liu, Carbon dioxide reforming of methane over Ni/Al_2O_3 treated with glow discharge plasma, Catal. Today 115 (2006) 205–210.
[36] T.J. Keskitalo, M.K. Veringa Niemelä, A.O.I. Krause, Modeling of the adsorption and desorption of CO_2 on Cu/ZrO_2 and ZrO_2 Catalysts, Langmuir 23 (2007) 7612–7619.
[37] M.C. Valero, P. Raybaud, P. Sautet, Interplay between molecular adsorption and metal–support interaction for small supported metal clusters: CO and C_2H_4 adsorption on Pd_4/γ-Al_2O_3, J. Catal. 247 (2007) 339–355.
[38] D. Mei, Q. Ge, J.H. Kwak, D.H. Kim, J. Szanyi, C.H.F. Peden, Adsorption and formation of BaO overlayers on γ-Al_2O_3 Surfaces, J. Phys. Chem. C 112 (2008) 18050–18060.
[39] O. Mekasuwandumrong, P.L. Silveston, P. Praserthdam, M. Inoue, V. Pavarajarn, W. Tanakulrungsank, Synthesis of thermally stable micro spherical χ-alumina by thermal decomposition of aluminum isopropoxide in mineral oil, Inorg. Chem. Commun. 6 (2003) 930–934.
[40] C. Meephoka, C. Chaisuk, P. Samparnpiboon, P. Praserthdam, Effect of phase composition between nano γ- and χ-Al_2O_3 on Pt/Al_2O_3 catalyst in CO oxidation, Catal. Commun. 9 (2008) 546–550.
[41] L. Cheng, Q. Ge, Effect of BaO morphology on NO_x abatement: NO_2 interaction with unsupported and γ-Al_2O_3-supported BaO, J. Phys. Chem. C 112 (2008) 16924–16931.
[42] D.H. Mei, V.A. Glezakou, V. Lebarbier, L. Kovarik, H.Y. Wan, K.O. Albrecht, M. Gerber, R. Rousseau, R.A. Dagle, Highly active and stable $MgAl_2O_4$-supported Rh and Ir catalysts for methane steam reforming: a combined experimental and theoretical study, J. Catal. 316 (2014) 11–23.
[43] I.N. Remediakis, F. Abild-Pedersen, J.K. Nørskov, DFT study of formaldehyde and methanol synthesis from CO and H_2 on Ni(111), J. Phys. Chem. B 108 (2004) 14535–14540.
[44] M. Rothaemel, H.W. Zanthoff, M. Baerns, Formation of CHO during interaction of CO and H_2 on alumina-supported Pd catalysts, Catal. Lett. 28 (1994) 321–328.
[45] M.A. Vannice, R.L. Garten, Supported palladium catalysts for methanation, Ind. Eng. Chem. Prod. Res. Dev. 18 (1979) 186–191.
[46] Y.X. Pan, C.J. Liu, Q.F. Ge, Effect of surface hydroxyls on selective CO_2 hydrogenation over Ni_4/γ-Al_2O_3: a density functional theory study, J. Catal. 272 (2010) 227–234.
[47] R.G. Zhang, B.J. Wang, H.Y. Liu, L.X. Ling, Effect of surface hydroxyls on CO_2 hydrogenation over Cu/γ-Al_2O_3 catalyst: a theoretical study, J. Phys. Chem. C 115 (2011) 19811–19818.
[48] R.G. Zhang, H.Y. Liu, B.J. Wang, L.X. Ling, Insights into the effect of surface hydroxyls on CO_2 hydrogenation over Pd/γ-Al_2O_3 catalyst: a computational study, Appl. Catal. B: Environ. 126 (2012) 108–120.
[49] Y. Choi, P. Liu, Mechanism of ethanol synthesis from syngas on Rh(111), J. Am. Chem. Soc. 131 (2009) 13054–13061.
[50] Y.H. Zhao, K.J. Sun, X.F. Ma, J.X. Liu, D.P. Sun, H.Y. Su, W.X. Li, Carbon chain growth by formyl insertion on rhodium and cobalt catalysts in syngas conversion, Angew. Chem. Int. Ed. 50 (2011) 5335–5338.
[51] M. Digne, P. Sautet, P. Raybaud, P. Euzen, H. Toulhoat, Use of DFT to achieve a rational understanding of acid–basic properties of γ-alumina surface, J. Catal. 226 (2004) 54–68.
[52] J.D. Li, C. Eric t, R.S. Luis, Effect of metal-support interface furring CH_4 and H_2 dissociation on Ni/γ-Al_2O_3: a density functional theory study, J. Phys. Chem. C 117 (2013) 16907–16920.
[53] Y.X. Pan, C.J. Liu, Q.F. Ge, Adsorption and protonation of CO_2 on partially hydroxylated γ-Al_2O_3 Surfaces: a density functional theory study, Langmuir 24 (2008) 12410–12419.
[54] M.C. Valero, M. Digne, P. Sautet, P. Raybaud, DFT study of the interaction of a single palladium atom with γ-alumina surfaces: the role of hydroxylation, Oil Gas Sci. Technol. 61 (2006) 535–545.
[55] G. Paglia, C.E. Buckley, A.L. Rohl, B.A. Hunter, R.D. Hart, J.V. Hanna, L.T. Byrne, Tetragonal structure model for boehmite-derived γ-Alumina, Phys. Rev. B 68 (2003) (144110-1-11).
[56] E. Menendez-Proupin, G. Gutierrez, Electronic properties of bulk γ-Al_2O_3, Phys. Rev. B 72 (2005) 035116-1-9.
[57] G. Paglia, C.E. Buckley, A.L. Rohl, Examination of spinel and nonspinel structural models for γ-Al_2O_3 by DFT and rietveld refinement simulations, J. Phys. Chem. B 110 (2006) 20721–20723.
[58] G. Paglia, E.S. Božin, S.J.L. Billinge, Fine-scale nanostructure in γ-Al_2O_3, Chem. Mater. 18 (2006) 3242–3248.

[59] Y.X. Pan, C.J. Liu, T.S. Wiltowski, Q.F. Ge, CO_2 adsorption and activation over γ-Al_2O_3-supported transition metal dimers: a density functional study, Catal. Today 147 (2009) 68–76.
[60] S.X. Yin, T. Swift, Q.F. Ge, Adsorption and activation of CO_2 over the Cu–Co catalyst supported on partially hydroxylated γ-Al_2O_3, Catal. Today 165 (2011) 10–18.
[61] H.T. Wang, L.J. Chen, Y.K. Lv, R.P. Ren, H_2 dissociation on γ-Al_2O_3 supported Cu/Pd atoms: a DFT investigation, Appl. Surf. Sci. 290 (2014) 154–160.
[62] A.A. Tsyganenko, P.P. Mardilovich, Structure of alumina surfaces structure of alumina surfaces, J. Chem. Soc. Faraday Trans. 92 (1996) 4843–4852.
[63] X.R. Shi, D.S. Sholl, Nucleation of Rh_n (n = 1–5) clusters on γ-Al_2O_3 surfaces: a density functional theory study, J. Phys. Chem. C 116 (2012) 10623–10631.
[64] B. Delley, From molecules to solids with the $DMol^3$ approach, J. Chem. Phys. 113 (2000) 7756–7764.
[65] B. Delley, An all-electron numerical method for solving the local density functional for polyatomic molecules, J. Chem. Phys. 92 (1990) 508–517.
[66] N. Govind, M. Petersen, G. Fitzgerald, D. King-Smith, J. Andzelm, A generalized synchronous transit method for transition state location, Comput. Mater. Sci. 28 (2003) 250–258.
[67] T.A. Halgren, W.N. Lipscomb, The synchronous-transit method for determining reaction pathways and locating molecular transition states, Chem. Phys. Lett. 49 (1977) 225–232.
[68] J. Greeley, M. Mavrikakis, A first-principles study of surface and subsurface H on and in Ni(111): diffusional properties and coverage-dependent behavior, Surf. Sci. 540 (2003) 215–229.
[69] S.S. Chuang, R.W. Stevens, R. Khatri, Mechanism of C_{2+} oxygenate synthesis on Rh catalysts, Top. Catal. 32 (2005) 225–232.
[70] J.J. Spivey, A. Egbebi, Heterogeneous catalytic synthesis of ethanol from biomass-derived syngas, Chem. Soc. Rev. 36 (2007) 1514–1528.
[71] N. Kapur, J. Hyun, B. Shan, J.B. Nicholas, K. Cho, Ab initio study of CO hydrogenation to oxygenates on reduced Rh terraces and stepped surfaces, J. Phys. Chem. C 114 (2010) 10171–10182.